American Mineralogist, Volume 69, pages 499–512, 1984

The Mg_2SiO_4 polymorphs (olivine, modified spinel and spinel)–thermodynamic properties from oxide melt solution calorimetry, phase relations, and models of lattice vibrations

MASAKI AKAOGI,[1] NANCY L. ROSS, PAUL MCMILLAN, AND ALEXANDRA NAVROTSKY

Departments of Chemistry and Geology
Arizona State University, Tempe, Arizona 85287

Abstract

High temperature solution calorimetry of the α-, β-, and γ-Mg_2SiO_4 polymorphs gives ΔH°_{1000} ($\alpha \rightarrow \beta$) = 7610±680 cal mol^{-1} and ΔH°_{1000} ($\beta \rightarrow \gamma$) = 1630±900 cal mol^{-1}. Based on the phase equilibrium data of Suito (1977) and appropriate thermal expansivity, compressibility, and heat capacity data, $\Delta S^\circ_{1000} = -2.5\pm0.5$ and -1.5 ± 0.9 cal mol^{-1} K^{-1} for the $\alpha \rightarrow \beta$ and $\beta \rightarrow \gamma$ transitions, respectively. Infrared and Raman spectra have been obtained for the three phases, and the lattice vibrational thermodynamic properties of the Mg_2SiO_4 polymorphs have been calculated using the model approach developed by Kieffer (1979c). A range of models consistent with the infrared and Raman data and compressional and shear wave velocities give entropies and heat capacities consistent with reported heat capacities (available only at 350–700 K for β- and γ-Mg_2SiO_4) and with the entropies of transition calculated above. From the vibrational calculations ΔS°_{1000} ($\alpha \rightarrow \beta$) = -2.8 ± 0.6 cal mol^{-1} K^{-1} and ΔS°_{1000} ($\beta \rightarrow \gamma$) = -1.3 ± 0.9 cal mol^{-1} K^{-1}. These two approaches to calculating ΔS° (calorimetry plus phase equilibria compared to vibrational calculations) offer means of constraining the P–T slopes of phase transitions at very high pressure, where experimental determinations suffer from serious uncertainties. The thermochemical data for α, β, and γ-Mg_2SiO_4 are used to construct the P,T diagram for these phases. The slopes of the α–β, β–γ, and α–γ boundaries are calculated to be positive and a triple point is predicted to be near 500 (±150) K and 120 (±10) kbar.

Introduction

At pressures and temperatures characteristic of the earth's mantle, common silicate minerals transform to denser phases. Thus in the range 130–160 kbar, forsterite (α-Mg_2SiO_4 with the olivine structure) transforms first to a modified spinel (β) and then to a spinel phase (γ). The detailed study and characterization of such materials is hampered by several problems. The apparatus to reach and control pressures of 100–200 kbar and temperatures of 1000–2000 K is costly to build and operate and generally produces only microgram to milligram quantities of sample. The calibration of pressure and temperature when both are high still has considerable uncertainties. The phases produced may not quench readily to ambient conditions for certain compositions, while for other samples the transformations at high pressure and temperature may be sluggish. Thus although high pressure phase equilibria have been mapped out roughly, the exact location of phase boundaries in P,T space and the proper reversal of reactions to demonstrate equilibrium remain largely unattained. Even when high pressure phases can be retained at ambient conditions, they are seldom available in suitable quantity for complete conventional thermodynamic characterization. For example, the measurement of low temperature heat capacity, necessary to calculate the standard entropy of a phase, requires on the order of 1 g or more of sample, making such a study prohibitive for a material synthesized a milligram at a time.

Because of the difficulties and uncertainties described above, it is desirable to constrain the thermodynamic properties of high pressure phases by as many independent lines of evidence as possible. In previous work (Navrotsky, 1973; Navrotsky et al., 1979) we have shown that high temperature solution calorimetry using molten $2PbO \cdot B_2O_3$ as solvent can measure enthalpies of the olivine–spinel transition in Ni_2SiO_4, Co_2SiO_4, and Fe_2SiO_4 using samples consisting of about 200 mg in total. Such enthalpies can then be used to constrain the pressure–temperature slopes of high pressure phase transitions and offer supporting evidence that the measured phase boundaries in the 30–80 kbar range reasonably approximate equilibrium.

The present work extends these calorimetric studies to

[1] Permanent address: Department of Earth Sciences, Kanazawa University, Kanazawa 920, Japan.

0003–004X/84/0506–0499$02.00

the Mg_2SiO_4 polymorphs. Because of the higher pressure required for their synthesis, these are available in even more limited supply than the corresponding iron, nickel and cobalt silicates, while at the same time their phase relations are more uncertain. The calorimetric data and observed pressures and volume changes of transformation are used to place bounds on the entropy changes and P–T slopes of the α–β and β–γ boundaries. At the same time, the entropies of transition are approached using another method, namely modelling of the vibrational contribution to the heat capacity, using newly measured infrared and Raman spectra and the approximations pioneered by Kieffer (1979c). The overall consistency of the entropies obtained using these two approaches (calorimetry plus phase equilibria compared to vibrational models) puts tighter constraints on values of $\Delta S°$ for the transitions than does either approach alone and suggests that such vibrational calculations may be useful for phases about which we have even less reliable thermodynamic information, e.g., the post-spinel phases in the system MgO–SiO_2, $MgSiO_3$ ilmenite and perovskite.

Experimental procedure

Sample synthesis and characterization

Mg_2SiO_4 olivine (about 5 g) was synthesized from an intimate mixture of MgO and silicic acid heated at 1573 K for 112 hr. Powder X-ray diffraction, microscopic observation and its Raman and infrared spectra indicated that the synthesized sample was single phase α-Mg_2SiO_4.

A reactive forsterite was used as a starting material for synthesis of β-Mg_2SiO_4 because the transition of well crystallized forsterite to β-phase is sluggish. A gel with Mg/Si = 2 was precipitated by mixing an alcoholic solution of ethyl orthosilicate and an aqueous solution of magnesium nitrate. The precipitated gel was heated at 1123 K for 127 hr. Powder X-ray diffraction data of the sample thus prepared showed the presence of very fine grained forsterite (~80%) and unreacted periclase plus silica (~20%). The stoichiometric Mg/Si ratio of 2 of this starting material was confirmed by electron microprobe analysis of the forsterite sintered at high pressure and high temperature from this starting material. High-pressure high-temperature syntheses were made using a double-stage, cubic-octahedral-anvil apparatus in the University of Tokyo, Japan. The starting material was put directly into a platinum cylindrical furnace, and was held at 145 kbar and 1123 K for 1 hr. The quenched sample was examined by powder X-ray diffraction and microscopic observation. It was well crystallized β-Mg_2SiO_4 (~200 mg) with very small amounts of forsterite (<1%) and platinum (~0.1%).

The γ-phase used in this work was kindly provided by Dr. E. Ito. For synthesis of the γ-Mg_2SiO_4, a uniaxial split-sphere type high-pressure apparatus in Okayama University, Misasa, Japan, was used. The starting material (forsterite) was put into a cylindrical platinum heater and was held at 220 kbar and 1473 K for 1 hr. The sample was quenched and examined by powder X-ray diffraction and microscopic observation. The product (~30 mg) was well crystallized γ-Mg_2SiO_4 with a small amount (<2% total) of $MgSiO_3$ perovskite and periclase.

Calorimetry

High-temperature solution calorimetric techniques in this study were the same as those described previously (Navrotsky, 1977). A twin Calvet-type microcalorimeter was used to measure enthalpies of solution of three polymorphs of Mg_2SiO_4 in molten $2PbO \cdot B_2O_3$ at 975 K. For the calorimetry of α-Mg_2SiO_4, incomplete dissolution was a problem in the initial runs using a solid-bottomed sample cup. Therefore sample containers with perforated platinum foil bottoms described by Navrotsky et al. (1980) were used. A thin platinum foil bottom, perforated with about 50 holes of diameters less than 80 μm, was attached to the platinum sample holder to form a miniature colander. The grains of α-Mg_2SiO_4 were sized not to pass through the holes. By using this cup with several rapid stirrings during the first few minutes, the α-Mg_2SiO_4 was dissolved rapidly and completely.

Metastability of β-Mg_2SiO_4 and γ-Mg_2SiO_4 in the calorimeter at 975 K was examined after equilibration for 5 hours. Both powder X-ray diffraction and microscopic observation indicated no evidence of back-transformation in the β-phase. However, the powder X-ray diffraction pattern of the heated γ-Mg_2SiO_4 showed weak reflections of α-Mg_2SiO_4 together with strong peaks of the γ-phase suggesting the beginning of back-transformation. Microscopic observation revealed a relatively small amount of highly birefringent material with refractive index lower than 1.68 plus a large amount of isotropic material with refractive index of 1.703 ± 0.006. The optical properties of both phases clearly indicated that the former was α-Mg_2SiO_4, while the latter was γ-Mg_2SiO_4. The amount of α-Mg_2SiO_4 in the heated γ-phase was estimated to be $10 \pm 5\%$ from its volume by microscopic observation. To minimize any effect of this back-transformation on the heats of solution, the equilibration time of the γ-Mg_2SiO_4 in the calorimeter prior to the solution run was reduced to 3 hours, and the observed heat of solution of the γ-phase was corrected for the 10% α-Mg_2SiO_4 present in the sample (see Table 1). Although no back-transformation of β-Mg_2SiO_4 was observed, the time of equilibration was also reduced to 3–5 hours. Both β- and γ-Mg_2SiO_4 were dissolved rapidly and completely in the flux. As described previously, the β-phase and γ-phase contained small amounts of phases other than the Mg_2SiO_4 polymorphs (<1% and <2%, respectively). No correction was made for these because their amounts were small and the heat of solution of $MgSiO_3$ perovskite is unknown.

Infrared and Raman spectroscopy

Near infrared powder transmission spectra were run in KBr discs between 300 and 1400 cm^{-1} using a Nicolet MX-1 interferometer. The amount of sample in each disc was 3.0 mg for 250 mg KBr. Far-infrared spectra were obtained with a Perkin-Elmer 180 spectrophotometer in the laboratory of Dr. George Rossman at the California Institute of Technology. Small amounts of specimen powder (2.0–3.0 mg) were mixed with Vaseline petroleum jelly on polyethylene plates. Scanning speed was variable, generally from 5 to 10 cm^{-1}/min and the slit width was also variable. Raman spectra were obtained by glancing angle reflection from a wall or pellet of powdered sample, using the 4880 or 5145Å line of a Spectra-Physics 171 argon laser, and a Spex 1402 double monochromator equipped with an RCA photomultiplier and photon-counting electronics. Laser power at the sample was 100–200 mW for the high-pressure phases to avoid overheating the samples. Slit widths were near 2 cm^{-1}.

Table 1. Enthalpies of solution of Mg_2SiO_4 polymorphs in $2PbO \cdot B_2O_3$ at 975 K

Sample weight (mg)	ΔH°_{sol} (cal mol^{-1})	
α-Mg_2SiO_4		
31.19	15447	
25.90	15263	
26.08	16406	
22.23	15867	
24.40	16617	
15.11	16815	
17.28	16074	
18.52	15865	
Average	16044 (8)	s(data) = 546[a] s(mean) = 193
β-Mg_2SiO_4		
15.99	8496	
14.92	9201	
14.49	8488	
15.35	8590	
13.69	9111	
13.83	9397	
Average	8881 (6)	s(data) = 402 s(mean) = 164
γ-Mg_2SiO_4		
14.82	8554	
7.73	7705	
Average	8130 ± 425 (2)	s(data) = 425
Average (corrected for 10% α)	7251 ± 700	

[a] number in parentheses is number of runs, s(data) is standard deviation of the data, s(mean) is standard deviation of the mean. 1 cal = 4.184 joule.

Thermochemical results and discussion

Calorimetric data

Enthalpies of solution of the olivine, modified spinel and spinel phase of Mg_2SiO_4 are shown in Table 1. Note that throughout this paper, calories are used; 1 cal = 4.184 joule. To calculate the enthalpy of solution of pure γ-Mg_2SiO_4, the observed enthalpy of solution was corrected for the presence of 10% olivine. The heat of solution of α-Mg_2SiO_4 shown in Table 1 is consistent with values measured by Charlu et al. (1975) and Wood and Kleppa (1981) within experimental error. Using the data in Table 1, the standard enthalpies at 975 K for the transitions among α-, β- and γ-Mg_2SiO_4 were calculated and are shown in Table 2 together with the data for the α–β–γ transitions in Co_2SiO_4 obtained previously (Navrotsky et al., 1979). Table 2 also contains the volume changes at 298 K and the calculated entropy changes, which will be discussed below in detail.

Note that the runs on β-Mg_2SiO_4 and on γ-Mg_2SiO_4 used totals of 88 and 23 mg, respectively, and that each run generally used about 15 mg. The results show a standard deviation of the data of about 400 cal, or a standard deviation of the mean of less than 200 cal. Thus reliable enthalpy of solution data can be obtained using the small amounts of sample available through high pressure synthesis.

Calculation of phase relations

From the enthalpy changes in Table 2, we can calculate slopes of the phase boundaries based on the Clausius–Clapeyron relation. To locate the phase boundaries in *P–T* space, the standard free energy of the transition at atmospheric pressure or the equilibrium transition pressure at the same temperature is required. For accurate calculations of the *P–T* slopes of the phase boundaries, the effects of compression and thermal expansion must be included. In the previous paper (Navrotsky et al., 1979), the phase boundaries were calculated including the effect of compression and thermal expansion but using the approximation of constant standard enthalpy and entropy changes for the transitions. In this work we adopt a better approximation in which the temperature dependence of enthalpy and entropy of transition is included by using the heat capacity data recently reported by Watanabe (1982). First, the effect of compression at a desired pressure and 298 K is calculated using a Murnaghan equation. Next, using X-ray and dilatometric data obtained at high temperature and one atmosphere, the molar volume is fitted as a linear function of temperature (a good fit between 300 and 1200 K and a reasonably reliable extrapolation to higher temperature). This results in the equation,

$$V_{T,P} = [V^\circ_{298} + a'(T - 298)] \cdot [PK'/K + 1]^{-1/K'} \quad (1)$$

in which V°_{298} is the molar volume at 298 K and 1 atm, a′ is a constant related to the thermal expansion coefficient, K and K' are the bulk modulus and its pressure derivative respectively, P is the pressure in kbar and T is the absolute temperature. This formalism approximates the effects of pressure and temperature as separate contributions. As discussed previously (Navrotsky et al., 1979)

Table 2. Thermochemical data for phase transitions among Mg_2SiO_4 and Co_2SiO_4 polymorphs

Compound		ΔV°_{298} (cm³ mol^{-1})	ΔH°_{1000} (cal mol^{-1})	ΔS°_{1000} (cal mol^{-1} K^{-1})
	α+β			
Mg_2SiO_4		-3.13[a]	7160 ± 680[a]	-2.5 ± 0.5[a], -2.8 ± 0.6[c]
Co_2SiO_4[b]		-2.90[b]	2150 ± 390[b]	-2.16 ± 0.3[b]
	β+γ			
Mg_2SiO_4		-0.89[a]	1630 ± 900[a]	-1.5 ± 0.9[a], -1.3 ± 0.9[c]
Co_2SiO_4		-1.02[b]	540 ± 430[b]	-0.98 ± 0.3
	α+γ			
Mg_2SiO_4		-4.02[a]	8790 ± 890[a]	-4.0 ± 0.7[a], -4.1 ± 1.0[c]
Co_2SiO_4		-3.92[b]	2690 ± 300[b]	-3.14 ± 0.3[b]

[a] this work, based on calorimetry and phase equilibria. 1 cal = 4.184 joule.
[b] Navrotsky et al. (1979).
[c] this work, based on vibrational calculations.

Table 3. Parameters used in phase diagram calculations

Compound	V^0_{298} ($cm^3\ mol^{-1}$)	a' ($cm^3\ mol^{-1}\ K^{-1}$)	K_0 (kbar)	K_0'	$C_p = a + bT + cT^{-2}$ (cal $mol^{-1}\ K^{-1}$)[j]		
					a	$bx10^3$	$c \times 10^{-5}$
α-Mg_2SiO_4	43.67[a]	0.00162[d,k]	1290[g]	5.2[g]	37.25	5.313	- 9.786
β-Mg_2SiO_4	40.54[a,b]	0.00128[e,k]	1660[h]	4[i]	36.29	5.519	-10.309
γ-Mg_2SiO_4	39.65[a,c]	0.00104[f,k]	2130[h]	4[i]	37.41	3.457	-11.436

a. Jeanloz and Thompson (1983), b. Akimoto et al. (1976), c. Ito et al. (1974), d. Hazen (1976), Smyth and Hazen (1973), Suzuki (1979), e. Suzuki et al. (1980), f. Suzuki et al. (1975), g. Graham and Barsch (1969), Kumazawa and Anderson (1969), h. Mizukami et al. (1975), i. Assumed, j. Watanabe (1982) (1 cal = 4.184 joule, k. calculated by fitting straight line to molar volume as function of temperatue (T in K) using indicated data, see text.

this relatively crude approximation is useful when more complete data on thermal expansion and compressibility at various T and P are lacking, as for β- and γ-Mg_2SiO_4. Using the heat capacities, changes of enthalpy and entropy for the transition with temperature are calculated by the following equations

$$\Delta H^\circ_T = \Delta H^\circ_{T_0} + \int_{T_0}^{T} \Delta C_P \, dT \qquad (2)$$

$$\Delta S^\circ_T = \Delta S^\circ_{T_0} + \int_{T_0}^{T} \frac{\Delta C_P}{T} \, dT \qquad (3)$$

where ΔH°_T and ΔS°_T are the enthalpy and entropy of transition, respectively at temperature T and atmospheric pressure, T_0 is the temperature of calorimetry, and ΔC_P is the heat capacity difference at T and 1 atm. The standard free energy of transition is then given by

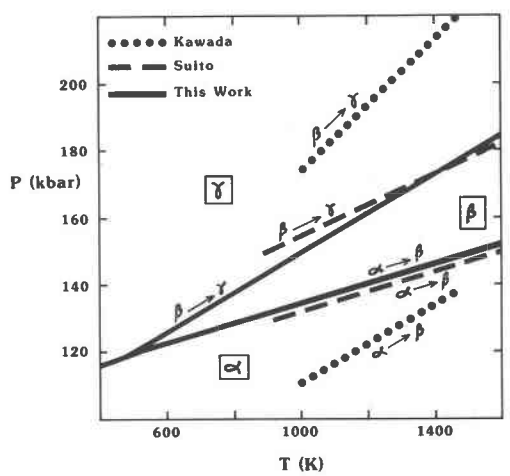

Fig. 1. Pressure–temperature relations for the Mg_2SiO_4 polymorphs. Solid lines are this work, parameters in Tables 2 and 3, discussion in text. Dotted and dashed boundaries are from Kawada (1977) and Suito (1977) respectively.

$$\Delta G_T = \Delta H^\circ_T - T\Delta S^\circ_T + \int_{1\ atm}^{P} \Delta V_{T,P} \, dP \qquad (4)$$

in which $\Delta V_{T,P}$ is the volume change for the transition calculated from equation (1). At equilibrium along the phase boundary

$$\Delta G_T = 0 \qquad (5)$$

Therefore, by using ΔH°_{975} and one P,T point on the phase boundary, together with $V^\circ(T)$, K, K' and C_P of the phases involved, we can calculate the phase boundary in the P–T space and also examine the sensitivity of the calculated boundary to the parameters. The parameters used in the calculations are listed in Table 3.

Two significantly different versions of the high pressure relations among α-, β-, and γ-Mg_2SiO_4 have been presented by Suito (1977) and by Kawada (1977). As shown in Figure 1, the transition pressure of Suito's boundary for the α–β transition, [P (kbar) = 98 + 0.035 T (K)] is ~15–20 kbar higher than that of Kawada's boundary, [P (kbar) = 43 + 0.068 T (K)]. Also the slope of Kawada's α–β boundary is about two times larger than Suito's. When Suito's transition pressure at 975 K is used with the enthalpy of α–β transition in Table 2, the calculated slope (0.027 kbar K^{-1}) is rather consistent with Suito's slope. However, if Kawada's transition pressure at 975 K is used, the calculated slope (0.003 kbar K^{-1}) is inconsistent with Kawada's value. To compare the calculated boundary with Suito's experimental results in more detail, the results of runs by Suito (1977) and the calculated phase boundaries from the thermochemical data are shown in Figure 2. In the calculation of the calorimetric phase boundaries, the transition point of 143 kbar and 1273 K on Suito's boundary was chosen, because, at that temperature, reaction rates probably would be fast enough for the observed transition pressure to approximate the equilibrium pressure. Suito's data permit a range of slope for the boundary. Calculated phase boundaries with three different slopes in the allowable range, consistent with the uncertainty in the calorimetric enthalpy of transition, are

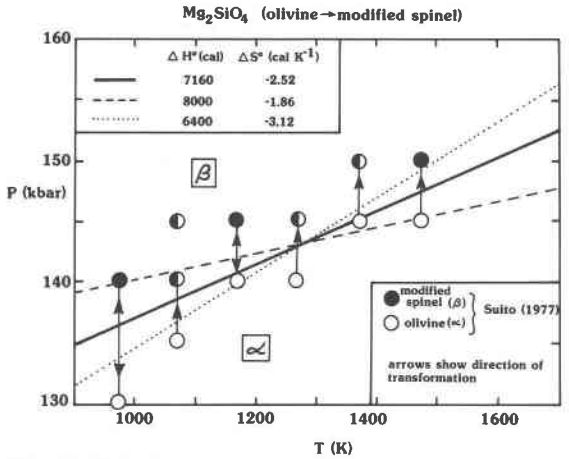

Fig. 2. Calculated phase boundary for $\alpha \rightarrow \beta$ Mg_2SiO_4 transition compared to experimental data (points) of Suito (1977). Solid line indicates best estimate of thermochemical parameters (calculations described in text), dashed and dotted lines represent extreme values of ΔH°, ΔS° allowed by calorimetric data and (P,T) point at 1273 K.

shown in Figure 2. The calculated values of ΔS°_{1000} corresponding to these three boundaries are also shown in the figure. Figure 2 shows that the thermochemical data for the α–β transition in Mg_2SiO_4 (ΔH°_{1000} = 7160±680 cal/mol, $\Delta S^\circ_{1000} = -2.5 \pm 0.5$ cal mol^{-1} K^{-1}), listed in Table 2, completely satisfy Suito's experimental results.

One may consider the sources of the discrepancy in the α–β boundary between the data of Suito (1977) and of Kawada (1977). A probable cause is the difference of pressure calibration at high temperatures, which is related to differences in the high-pressure apparatus used in their studies. Using the coesite–stishovite boundary of Yagi and Akimoto (1976), Suito found virtually no difference between pressures at 90–100 kbar and 873–1473 K, and those calibrated at room temperature in his experiments using a uniaxial split-sphere high-pressure apparatus. However, in Kawada's work, using a Bridgman-anvil apparatus, a large pressure correction was inferred from calibration near 1273 K and 90–100 kbar. Uncertainties in this correction may be large enough to account for the differences in both absolute values of pressure and in P–T slopes. As shown in Figure 1, thermochemical data obtained in this study are quite consistent with Suito's results, but not with Kawada's.

Very recently, Fukizawa (1982) determined the α–β transition pressure in Mg_2SiO_4 by means of high-pressure high-temperature experiments using an in-situ X-ray diffraction method, in which pressure values were measured based on a gold pressure standard. Although his data are still preliminary, a combination of the enthalpy of transition obtained in our work with an accurately determined P,T point, based on in-situ X-ray diffraction experiments at high pressures and high temperatures, would provide further refinement of the phase boundary.

It is somewhat difficult to locate accurately the β–γ phase boundary calculated from the thermochemical data. In the β–γ transition, since ΔH° and ΔS° are small, the $\int_{1\text{ atm}}^{P} \Delta V_{T,P}\, dP$ term in equation (4) is of comparable magnitude to ΔH° and $T\Delta S^\circ$. Therefore, the errors in compressibilities, thermal expansivities and heat capacities of β- and γ-phase result in great uncertainties in $\Delta G(P,T)$. Furthermore, considerably different lattice parameters for β- and γ-Mg_2SiO_4 than those used in Tables 2 and 3 have been recently reported (Horiuchi and Sawamoto, 1981; Sasaki et al., 1982). The new cell volumes of β- and γ-phase result in a volume change ΔV°_{298} ($\beta \rightarrow \gamma$), of -1.02 cm^3 mol^{-1}, which is about 15% larger in magnitude than the -0.89 cm^3 mol^{-1}, listed in Table 2 and 3. In addition, the thermal expansion data of Suzuki et al. (1980) show considerable scatter and Sato (1970) suggested that the thermal expansivity of β-Co_2SiO_4 is smaller than that of γ-Co_2SiO_4. Thus considerable uncertainty exists in the value of ΔV ($\beta \rightarrow \gamma$). The solid line (curve 1) in Figure 3 is calculated with ΔH = 1630 cal mol^{-1}, $\Delta S = -1.5$ cal mol^{-1} K^{-1} and $\Delta V = -0.89$ cm^3 mol^{-1}, independent of P and T (as in Table 2). The points represent the phase transformation data of Suito (1977). Note that none of these points has been reversed so that they may represent synthesis rather than equilibrium

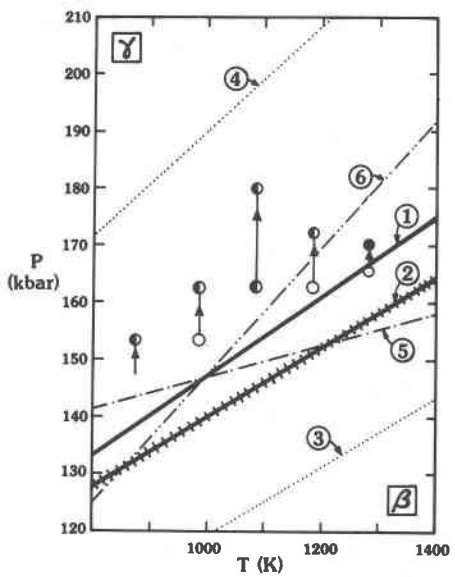

Fig. 3. The β–γ transition. Points represent experiments of Suito (1977). Solid line, curve 1, is "best" thermochemical calculation, with ΔH° = 1630 cal mol^{-1}, $\Delta S^\circ = -1.5$ cal mol^{-1} K^{-1}, $\Delta V^\circ = -0.89$ cm^3 mol^{-1}. Hatched line (curve 2) is experimental phase boundary quoted by Sawamoto (1983, personal communication). Other lines are calculated using values of ΔH° (cal mol^{-1}), ΔS° (cal mol^{-1} K^{-1}), ΔV° (cm^3 mol^{-1}) allowed by uncertainties in experimental data as follows: curve 3, ΔH° = 1630, $\Delta S^\circ = -1.5$, $\Delta V^\circ = -1.09$; curve 4, ΔH° = 1630, $\Delta S^\circ = -1.5$, $\Delta V^\circ = -0.69$; curve 5, ΔH° = 2530, $\Delta S^\circ = -0.6$, $\Delta V^\circ = -0.89$; curve 6, ΔH° = 730, $\Delta S^\circ = -2.4$, $\Delta V^\circ = -0.89$.

conditions. Indeed a β–γ boundary at somewhat lower pressures, shown by curve 2 in Figure 3, has been suggested from crystal growth experiments by Sawamoto (1983, pers. comm.). The calculated curve lies between these two determinations.

The lower and upper dotted lines (curves 3 and 4) show the effect of changing ΔV by ± 0.2 cm^3 mol^{-1} while keeping $\Delta H°$ and $\Delta S°$ constant. The dot-dashed and double-dot-dashed lines (curves 5 and 6) show the effect of varying $\Delta H°$ by the calorimetric uncertainty and adjusting $\Delta S°$ to keep $\Delta G°_{1000}$ constant, while keeping $\Delta V° = -0.89$ cm^3 mol^{-1}. Numerous other boundaries, generally falling between curves 3 and 4, can be generated by simultaneous variation of $\Delta H°$, $\Delta S°$, and $\Delta V°$ within limits consistent with the uncertainties in the calorimetric, X-ray, and phase boundary data. (Note that to maintain such consistency, variations, in $\Delta H°$, $\Delta S°$, and $\Delta V°$ can not be made completely independently of each other.) We conclude that the values of $\Delta H°$, $\Delta S°$, and $\Delta V°$ listed for the $\beta \rightarrow \gamma$ transition in Table 2 are consistent with the phase relations and thermochemical data as currently known, but tighter constraints on these parameters must await further study, including that of thermal expansion and compressibility.

Figure 1 summarizes the calorimetric boundaries of α–β–γ transitions in Mg_2SiO_4. The α–γ boundary was calculated from the data in Table 2. The calorimetric boundaries define a triple point at approximately 120 kbar and 500 K. The uncertainties in this value arising from uncertainties in the calculated P,T boundaries are of the order of ± 150 K and ± 10 kbar. The phase boundaries determined from the high pressure studies of Suito (1977) and Kawada (1977) also suggest a triple point, probably at somewhat lower temperature than that calculated from the thermochemical data.

Relation of thermochemical and structural parameters

$\Delta V°$, $\Delta H°$ and $\Delta S°$ for the α–β transition in Mg_2SiO_4 are 78, 81, and 63%, respectively, of the corresponding values for the α–γ transition. In the previous calorimetric study on the high-pressure polymorphs of Co_2SiO_4 (Navrotsky et al., 1979), quite similar results were obtained: $\Delta V°_{298}$, $\Delta H°$ and $\Delta S°$ for the α–β transition in Co_2SiO_4 are 74, 80 and 69%, respectively, of those for the α–γ transition. These results suggest that, on the basis of thermochemical properties, the β-phase resembles the spinel rather than olivine. The α–β–γ transition do not involve any changes in the coordination numbers of cations. However, the structures of β-phase and spinel are based on a slightly distorted cubic close packing of oxygen atoms, while the olivine structure is based on hexagonal close packing. Recent structural studies on β-Mg_2SiO_4 and γ-Mg_2SiO_4 reveal that a small increase of mean Si–O bond length and a decrease of average Mg–O distance are observed in the $\alpha \rightarrow \beta \rightarrow \gamma$ transitions, and that these changes are larger in the $\alpha \rightarrow \beta$ transition than in the $\beta \rightarrow \gamma$ transition (Horiuchi and Sawamoto, 1981; Sasaki et al., 1982). Similar results were obtained for the $\alpha \rightarrow \beta \rightarrow \gamma$ transitions in Co_2SiO_4 (Morimoto et al., 1974). Therefore, in terms of structural data, as well in terms of the thermochemical data presented here, the β-phase is more similar to spinel than to olivine for both Mg_2SiO_4 and Co_2SiO_4.

Vibrational spectra, models of lattice vibrations, and calculation of vibrational entropies

Vibrational spectra

The observed near- and far-infrared and Raman spectra for α-, β- and γ-Mg_2SiO_4 are shown in Figure 4 and the peaks are tabulated in Table 4. The infrared and Raman spectra for α-Mg_2SiO_4 (forsterite) are comparable to those of previous workers (Oehler and Gunthard, 1969; Servoin and Piriou, 1973; Iishi, 1978). Factor group analysis (e.g., Fateley et al., 1972) gives the number and symmetries of expected bands, summarized below for the three phases.

(a) α-Mg_2SiO_4: Space group *Pbnm*: Z = 4
Raman: 11 A_g + 7 B_{1g} + 11 B_{2g} + 7 B_{3g}
Infrared: 14 B_{1u} + 10 B_{2u} + 14 B_{3u}
Inactive: 10A_u
Acoustic: B_{1u} + B_{2u} + B_{3u}

(b) β-Mg_2SiO_4: Space group *Imma*: Z = 4 (for primitive cell)
Raman: 11 A_g + 7 B_{1g} + 9 B_{2g} + 12 B_{3g}
Infrared: 14 B_{1u} + 13 B_{2u} + 11 B_{3u}
Inactive: 7A_u
Acoustic: B_{1u} + B_{2u} + B_{3u}

(c) γ-Mg_2SiO_4: Space group F*d3m*: Z = 2 (for primitive cell)
Raman: A_{1g} + E_g + 3F_{2g}
Infrared: 4 F_{1u}
Inactive: F_{1g} + 2 A_{2u} + 2 E_u + 2 F_{2u}
Acoustic: F_{1u}

The infrared spectrum of γ-Mg_2SiO_4 shows a major band near 830 cm^{-1}, comparable to those for γ-Fe_2SiO_4, γ-Ni_2SiO_4 and γ-Co_2SiO_4 (Jeanloz, 1980). These last three phases also show distinct bands near 500 and 350 cm^{-1}, while the γ-Mg_2SiO_4 sample has only a single broad band centered near 445 cm^{-1} (Fig. 4), which may contain components corresponding to the two bands of the Fe-, Ni- and Co- phases. Assignment of these bands has been discussed by Jeanloz (1980). The 830 cm^{-1} band has marked shoulders near 930 and 790 cm^{-1}, while the 445 cm^{-1} band shows shoulders near 510 and 395 cm^{-1}, and two weak sharp features at 543 and 348 cm^{-1}. The 510 cm^{-1} shoulder may correspond to the band near 500 cm^{-1} observed for the Fe-, Ni- and Co- spinels by Jeanloz (1980). However, only four infrared bands are expected for γ-Mg_2SiO_4. The additional features could be due to some deviation of the spinel from cubic symmetry but none was indicated by the X-ray study of Sasaki et al.

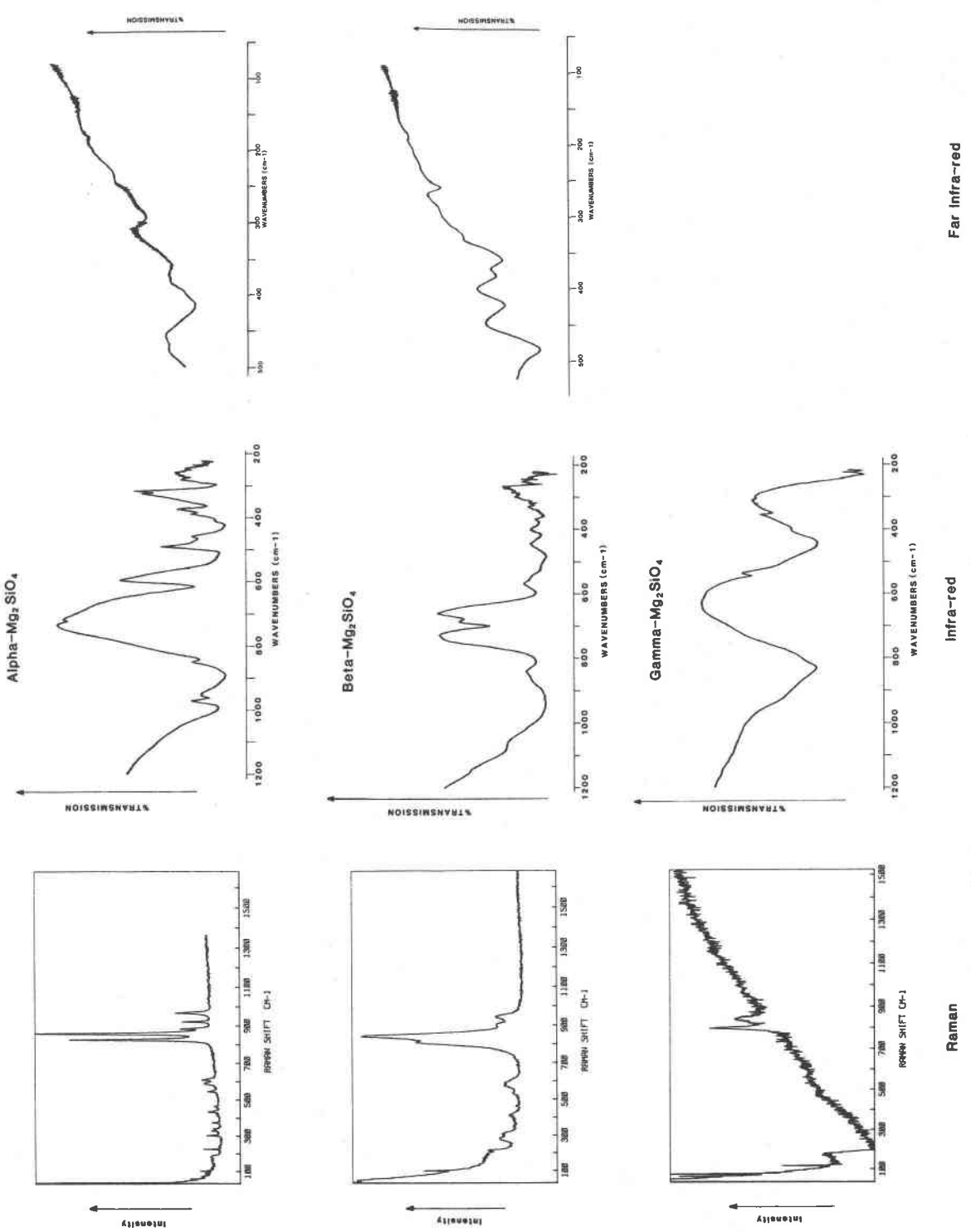

Fig. 4. Infrared and Raman spectra of α-, β- and γ-Mg_2SiO_4.

Table 4. Observed infrared and Raman bands for α-, β- and γ-Mg_2SiO_4

α-Mg_2SiO_4				β-Mg_2SiO_4		γ-Mg_2SiO_4	
Raman		Infrared		Raman	Infrared	Raman	Infrared
		135 ?	B_{2u}		130 ?		
163	B_{1g}						
					188		
180	A_g	184	$B_{1u}+B_{3u}$				
				213	208		
223	A_g	228	$B_{1u}+B_{2u}+B_{3u}$				
		268 sh	$B_{1u}+B_{3u}$		226		
300	A_g	293	$B_{1u}+B_{2u}+B_{3u}$				
312	$B_{1g}+B_{3g}$	318 ?	B_{3u}				
				280	288		
325	$B_{2g}+A_g$						
				307	316 ?sh		
336	A_g	336 sh	B_{3u}		326		
		360	$B_{1u}+B_{2u}$				
371	$B_{2g}+B_{3g}$	378 sh	B_{3u}		345 sh		350 w
					359		
		395 sh	$B_{2u}+B_{3u}$				
					381		
		416	$B_{1u}+B_{2u}$	408			395 sh
430	A_g+B_{1g}				422		
				460		455	445
438	B_{2g}				485		
							510 sh
460	B_{3g}	470	B_{1u} or B_{2u}	528	520		
						550	545 w
		480 sh	B_{1u}		550		
				570			
		510	$B_{1u}+B_{2u}$	588	595		
542	A_g	540 sh	B_{2u}		645 sh		
					675		
586	$B_{1g}+B_{2g}+B_{3g}$	570 sh	B_{3u}				
					700		
606	A_g	615	B_{3u}			781 A_g?	785 sh
				850 A_g?	805		
820	A_g	840	$B_{2u}+B_{3u}$				
				836 A_g?			830
853	A_g				855		
						877 F_{2g}?	
878	B_{2g}	870 sh	$B_{1u}+B_{2u}+B_{3u}$	898			920 sh
		890		919	910		
916	B_{3g}			940	945		
					985 sh		
962	A_g	960	B_{3u}		1080 sh		
					1150 sh		
		990	$B_{2u}+B_{3u}$				

Notes: All frequencies are in cm^{-1}. Infrared positions were estimated at the transmission minima. Band symmetry assignments for α-Mg_2SiO_4 are from Servoin and Piriou (1973) and Iishi (1978). Suggested assignments for β- and γ-Mg_2SiO_4 are from band intensities. The queried (?) bands at 135 and 130 cm^{-1} in the far infrared spectra of α- and β-Mg_2SiO_4 occur in a noisy part of the spectrum, but may be real. A band was observed at 144 cm^{-1} for α-Mg_2SiO_4 by Oehler and Gunthard (1969), and appeared in the calculation of Iishi (1978). Sh means shoulder, w means weak.

(1982), although some Mg–Si disorder was possible. Jeanloz (1980) observed similar shoulders on the major bands of γ-Fe_2SiO_4, γ-Ni_2SiO_4 and γ-Co_2SiO_4, which he attributed to some vibrational coupling between octahedral and tetrahedral cation site vibrations. No far-infrared spectrum was obtained for the γ-Mg_2SiO_4 sample, but studies of other silicate spinels suggest a further band below 400 cm^{-1} (White and DeAngelis, 1967). The Raman spectrum of γ-Mg_2SiO_4 (Fig. 4) shows two major bands at 781 and 877 cm^{-1}. These are probably respectively the A_{1g} and F_{2g} modes derived from ν_1 (symmetric) and ν_3 (asymmetric) stretching motions of the tetrahedral SiO_4 groups (see White, 1975; Piriou and McMillan, 1983). These are at lower frequency than the corresponding bands in α-Mg_2SiO_4, which may be related to the longer average Si–O distances in the spinel phase. Two further weak bands are observed near 455 and 550 cm^{-1}, but there is no indication of the remaining band expected in the Raman spectrum. The feature near 180 cm^{-1} is not part of the spectrum, but is due to a stray reflection within the spectrometer. The sharp spikes below 100 cm^{-1} are due to plasma lines of the laser and rotational bands of N_2 and O_2 in the air, while the steeply rising background is caused by fluorescence probably due to some trace impurity in the sample.

Jeanloz (1980) obtained the infrared spectrum of β-Co_2SiO_4. He noted a band at 686 cm^{-1}, which he assigned to a symmetric stretching vibration of the Si_2O_7 units present in the β-phase. We observe two bands at 700 and 675 cm^{-1} in the infrared spectrum of β-Mg_2SiO_4 (Fig. 4) which might be given the same assignment. However, no analogous bands are observed in the Raman spectrum for β-Mg_2SiO_4 (Fig. 4). The Si_2O_7 units in β-Mg_2SiO_4 have site symmetry C_{2v} within a crystal symmetry D_{2h}^{28} (Horiuchi and Sawamoto, 1981), with two Si_2O_7 units per spectroscopic unit cell. The symmetric stretching vibra-

tion about the bridging oxygen should give rise to two crystal bands with symmetries B_{2u} and A_g, one active in the infrared and the other strong in the Raman spectrum. We observe two bands in this region in the infrared spectrum and none in the Raman. From this, it is possible that a description in terms of discrete Si_2O_7 units may not be the best interpretation of the vibrational spectra of β-Mg_2SiO_4. It is of interest that both the infrared and Raman spectra of β-Mg_2SiO_4 are similar to those of α-Mg_2SiO_4. This is reasonable, since a similar number of bands with a similar distribution of symmetry species is predicted in the spectra of both (36 Raman and 38 infrared for α-Mg_2SiO_4; 39 Raman and 38 infrared for β-Mg_2SiO_4). Also the average bond lengths in both are similar (although Si–O is slightly longer and Mg–O shorter in β-Mg_2SiO_4) even though the structures are significantly different (Horiuchi and Sawamoto, 1981). The major high-frequency bands for β-Mg_2SiO_4 do occur at slightly lower frequency than for the α phase, which may be related to the slight expansion of the SiO_4 units in β relative to α-Mg_2SiO_4.

For the purposes of the present calculation of vibrational entropies, the observed infrared and Raman spectra have been simplified as described below. We note that a number of inactive modes is predicted for all three Mg_2SiO_4 polymorphs, while not all of the expected active modes have been observed, and that we have no information on the dispersion relations for these modes. These uncertainties limit the rigor with which the vibrational calculations can be performed but, as will be discussed below, useful results can still be obtained.

Kieffer's model

Entropies and heat capacities of the Mg_2SiO_4 polymorphs can be calculated with Kieffer's lattice vibrational model which provides an approximation of the real vibrational spectrum of a mineral (Kieffer, 1979a,b,c, 1980). The thermodynamic functions of a crystal can be expressed as averages over the vibrational density of states. These functions are relatively insensitive to the details of the spectrum, except at low temperature, so Kieffer's approximation generally yields good estimates of the heat capacities and entropies of minerals.

The Kieffer vibrational model takes the vibrational unit of a crystal as the primitive unit cell and has 3s total degrees of freedom associated with it (s = number of atoms in unit cell). Of the 3s degrees of freedom, only three are acoustic modes, namely two shear modes (S) and one longitudinal (P) mode characterized by acoustic velocities. A simple sine wave dispersion of these modes toward the edge of the Brillouin zone is assumed. The remaining 3s-3 modes are optic modes and span a broad range of frequencies. An estimate of the range is obtained from far-infrared, near-infrared and Raman spectra. Little information is available about dispersion of the optic modes across the Brillouin zone for most mineral phases. Since this is most critical for the lowest frequency mode which greatly affects C_P at low temperature, the lowest optic mode is assumed to vary inversely with a characteristic mass ratio across the Brillouin zone. The optic modes are distributed uniformly between a lower cutoff frequency, ω_l, and an upper cutoff frequency, ω_u, specified from spectral data. Any isolated modes (such as Si–O and O–H stretching modes) are represented as separate Einstein oscillators, designated by ω_{E1}, ω_{E2}, . . ., or by a second optic continuum. Thus the assumed frequency distribution is a sum of the acoustic branches, optic continuum(a) and Einstein oscillators. Data required for the model are acoustic velocities, crystallographic data and spectroscopic data.

General approach to vibration models

From the discussion above, it is clear that no unique model, incorporating an unequivocal assignment of vibrational modes and specific dispersion relations, can be selected for a complex silicate such as an Mg_2SiO_4 polymorph. Rather a set of related models with small differences in band assignments, partitioning of modes into optic continua and Einstein oscillators, and dispersion relations, can be developed for each phase such that these models are consistent with the observed spectra, acoustic velocities and constraints of crystallographic symmetry. In the sections which follow, we show that such a set of models for the Mg_2SiO_4 polymorphs yield heat capacities and entropies which cluster around (to 5% or better) measured heat capacities and entropies derived above from calorimetry and phase equilibria. Such models, shown in Table 5, are all approximately equally "good" in the sense that they are consistent with both the spectra and the thermochemical data, and we have no way of selecting any as significantly "better". The encouraging feature of these calculations is that, although no single model can be selected, the range of models consistent with spectroscopic data and showing reasonable dispersion relations give values of C_P and $S°$ which are relatively insensitive to the details of modelling. Using models with features generally inconsistent with the spectra give a much larger range of C_P and $S°$ values and such models will not be considered further except to note that simple Debye models consistently underestimate C_P and $S°$ by 10–20% (Watanabe, 1982).

The unknown vibrational parameters, including inactive modes and dispersion relations, clearly constitute a weak point of the modelling. Were these known, the vibrational modelling could proceed entirely independently of the known thermochemical data. However, without such knowledge, we have had to use the observed C_P and $\Delta S°$ values to put some bounds on the low frequency cutoff of the optic continuum, especially for γ-Mg_2SiO_4 which has the smallest number of bands active in the infrared and Raman.

The model treats each vibration as harmonic and gives

Table 5. Vibrational models for Mg_2SiO_4 polymorphs

Mineral	(0)[a] cm^{-1}	$\omega_{L1}(k_{max})$[b] cm^{-1}	ω_{U1}[c] cm^{-1}	m_2/m_1[d]	ω_{L2}[e] cm^{-1}	ω_{U2}[f] cm^{-1}	q_0[g]	ω_{E1}[h] cm^{-1}	q_1[i]	ω_{E2}[h] cm^{-1}	q_2[i]	ω_{E3}[h] cm^{-1}	q_3[i]	$S°$ (cal mol^{-1} K^{-1}) 298 K	700 K	1000 K	$C_p°$ (cal mol^{-1} K^{-1}) 298 K	700 K	1000 K
α-Mg_2SiO_4																			
Model 1	144	128	620	92/24				950	0.190					23.52	53.12	67.74	27.72	39.05	41.63
Model 2	144	128	620	92/24				837	0.048	930	0.142			23.75	53.48	68.60	28.14	39.27	42.35
Model 3	144	144	620	0/1.0				837	0.048	930	0.142			22.75	52.42	67.04	27.72	39.12	41.70
Model 4	144	128	620	92/24				900	0.095	1000	0.095			23.52	53.12	67.74	27.72	39.05	41.63
Model 5	144	128	620	92/24	850	950	0.19							23.52	52.70	66.90	27.58	38.83	40.44
β-Mg_2SiO_4																			
Model 1	190	167	590	84/24				700	0.025	950	0.210			21.14	50.18	64.68	26.85	38.70	41.37
Model 2	190	178	590	168/24				700	0.030	950	0.200			20.79	49.90	64.40	26.88	38.73	41.40
Model 3	190	178	600	168/24				700	0.050	810	0.095	950	0.095	20.58	49.90	64.47	27.02	38.94	41.51
Model 4	190	167	590	84/24	700	950	0.245							21.07	49.83	64.02	26.88	37.86	40.25
Model 5	190	167	590	84/24	920	950	0.210	700	0.035					20.86	49.34	63.42	26.46	37.58	40.11
γ-Mg_2SiO_4																			
Model 1	240	214	550	92/24				850	0.300					19.74	48.52	62.91	26.32	38.51	41.14
Model 2	240	194	520	46/24				850	0.340					20.30	48.87	63.26	26.11	38.44	41.07
Model 3	220	178	520	46/24				850	0.360					20.44	48.87	63.19	25.90	38.30	41.00
Model 4	260	232	550	92/24	830	850	0.200							20.79	49.22	62.84	27.16	36.90	38.90
Model 5	250	250	520	0/1.0	825	835	0.230							20.30	48.52	62.14	26.81	37.36	38.83

[a] Lower limit of first optic continuum (O.C.) at K = 0; [b] Lower limit of first O.C. at K_{max}; [c] Upper limit of first O.C.; [d] Mass ratio; [e] Lower limit of second O.C.; [f] Upper limit of second O.C.; [g] Modes partitioned in second O.C.; [h] Einstein oscillators (E.O.'s) 1,2 and 3; [i] Modes partitioned at E.O.'s 1,2 and 3.
1 cal = 4.184 joule.

C_v. We have included anharmonicity in the term converting C_V to C_P ($C_P - C_V = TV\alpha/\beta^2$). Though this does not entirely take care of possible anharmonic effects at $T >$ 1000 K (especially since $V(P,T)$ is poorly known), the generally good agreement with experimental thermochemical data suggests that such effects are probably relatively unimportant.

Details of vibrational models for the Mg_2SiO_4 polymorphs

Forsterite, α-Mg_2SiO_4. Forsterite is orthorhombic and belongs to space group *Pbnm* (Brown, 1980). The primitive unit cell contains four formula units. Thus the cell has 28 atoms and 84 degrees of freedom. The unit cell volume is 290.8×10^{-24} cm^3 and the radius of the Brillouin zone (approximated by a sphere) is 5.89×10^7 cm^{-1}.

Acoustic velocities for forsterite have been thoroughly studied and the following values were used in the model: ν_p = 8.56 km s^{-1}, ν_s = 4.93 km s^{-1} and ν_{max} = 5.00 km s^{-1} (Kieffer, 1980). The corresponding directionally averaged wave velocities are ν_1 = 4.90 km s^{-1}, ν_2 = 4.96 km s^{-1} and ν_3 = 8.56 km s^{-1} (Kieffer, 1979a). These velocities give acoustic branches that reach 89, 99 and 171 cm^{-1} at the Brillouin zone boundary.

Features of the forsterite spectra (Fig. 4) that should be noted for the lattice vibrational models are the two distinct bands of frequencies ranging from 144 to 620 cm^{-1} and 830 to 985 cm^{-1} Models for α-Mg_2SiO_4 which fit experimental $C_P°$ and $S°$ data (Orr, 1953; Robie et al., 1978; Watanabe, 1982) within 2–3% are presented in Table 5. All models have an optic continuum ranging from 144 cm^{-1} (lowest optical mode at k = 0) to 620 cm^{-1}. The high frequency bands which are due to [SiO_4] stretching vibrations can be represented by one Einstein oscillator, two oscillators or a second optic continuum. Using the partitioning method of Kieffer (1979b), 19% of the total degrees of freedom are assigned to these high frequency modes.

In the majority of models studied, the lower limit of the optic continuum at k = 0, 144 cm^{-1}, was dispersed to 128 cm^{-1} at the Brillouin zone boundary. The characteristic mass ratio of 92/24 corresponds to the assumption that the low frequency vibration can be described as a Mg atom vibrating against a [SiO_4] tetrahedron. A lattice dynamical calculation of forsterite by Iishi (1978) supports this assumption.

Models with the optic continuum extending from 620 cm^{-1} to 128 cm^{-1} at k_{max} show very good agreement with experimental heat capacity data. These models, however, tend to overestimate entropies slightly, implying that the lower limit of 128 cm^{-1} for the optic continuum is too low. An excellent fit to the entropy data can be obtained if the lowest optical mode at k = 0, 144 cm^{-1}, is not dispersed at all across the Brillouin zone (Table 5: α-Mg_2SiO_4, Model 3). However, the 144 cm^{-1} mode is not certain and has only been seen by Oehler and Günthard (1969). Our Far-infrared spectrum of α-Mg_2SiO_4 is not definitive in this region.

The distribution of modes in the far-infrared spectral region (at k_{max}) is critical in the calculation of entropies. $S°$ and $C_P°$ increase as the lower limit of the optic continuum at k = 0 is dispersed to lower values at k_{max}. Models for α-Mg_2SiO_4 in Table 5 demonstrate that $C_P°$ and $S°$ are much less sensitive to details of the high frequency part of the spectrum. Variation in the placement of Einstein oscillators and distribution of modes between oscillators have negligible effect upon $C_P°$ and $S°$. In addition, little difference in $C_P°$ and $S°$ is found whether one Einstein oscillator or two oscillators are used to model the high frequency [SiO_4] stretching modes. Finally, α-Mg_2SiO_4 can be modelled with two optic continua (Table 5: α-Mg_2SiO_4, Model 5). Model 5 shows generally good agreement with the heat capacity and entropy data.

Modified spinel, β-Mg_2SiO_4. Modified spinel, β-Mg_2SiO_4, is orthorhombic and belongs to space group *Imma* (Horiuchi and Sawamoto, 1981). The primitive unit cell, which is half the size of the conventional body-centered cell, has four formula units, 28 atoms and hence 84 degrees of freedom. The unit cell volume is 269.1×10^{-24} cm^3 and the Brillouin zone radius is 6.04×10^7 cm^{-1}.

Unlike those of forsterite, the acoustic velocities of β-Mg_2SiO_4 have not been thoroughly studied. Using data from germanate compounds analogous to the Mg_2SiO_4 polymorphs (Liebermann,

1973, 1975), the compressional and shear wave velocities of β-Mg_2SiO_4 were estimated to be ν_p = 9.6 km s^{-1} and ν_s = 5.4 km s^{-1}. These velocities give acoustic branches that reach 198 and 116 cm^{-1} at the Brillouin zone boundary. Features of the β-Mg_2SiO_4 spectra (Fig. 4) that should be noted for modelling are the lowest frequency band at 190 cm^{-1}, the continuous range of modes to 590–600 cm^{-1}, the band at 700 cm^{-1} and the higher frequency modes between 800 and 1100 cm^{-1}.

Experimental heat capacity and entropy data for β-Mg_2SiO_4 are much more limited than those for forsterite. In this investigation, two sources were used to provide data for comparison with model calculations: Watanabe's (1982) heat capacity data from 350–700 K obtained from differential scanning calorimetry and an estimate of S°_{1000} based on a combination of solution calorimetric experiments and phase equilibria studies of the Mg_2SiO_4 polymorphs (see above). One should note that Watanabe's (1982) heat capacity data for forsterite are systematically 1% higher than Orr's (1953) heat capacity data. This raises the possibility that Watanabe's heat capacities for β- and γ-Mg_2SiO_4 may likewise be systematically high. Thus a 3–4% difference between C°_P calculated from the models and measured by Watanabe may in fact represent good agreement between calculation and experiment, when errors in both are considered.

Models for β-Mg_2SiO_4 which show good agreement with the experimental data are presented in Table 5. These models all have a common feature—an optic continuum ranging from 590–600 to 190 cm^{-1} (at k = 0).

A number of different mass ratios were tried in dispersing the lowest optical mode at k = 0, 190 cm^{-1}, across the Brillouin zone to k_{max}. Mass ratios of 168/24 and 84/24 provided the best fit with experimental data. These mass ratios were obtained by assuming that a Mg atom vibrating against the $[Si_2O_7]$ cluster or part of the cluster is involved in the low frequency mode. With dispersion taken into account, the optic continuum is extended from 590 cm^{-1} to 178 cm^{-1} (for m_2/m_1 = 168/24) or 167 cm^{-1} (for m_2/m_1 = 84/24) at k_{max}. Models which disperse the low frequency mode lower than 167 cm^{-1} yield values inconsistent with observed C°_P and S° values. This offers support for not including the questionable 130 cm^{-1} band (Fig. 4 and Table 4) in the vibrational models for β-Mg_2SiO_4.

Enumeration of the silicon-oxygen stretching modes in β-Mg_2SiO_4 is more complex than in α-Mg_2SiO_4 because there are Si–O bridging (Si–O_{br}) as well as Si–O nonbridging (Si–O_{nbr}) bonds. Following the methodology presented by Kieffer (1980) for the chain silicates, each Si_2O_7 group has two Si–O_{br} and six Si–O_{nbr} bonds. Si–O_{br} bonds give rise to two symmetric and two antisymmetric vibrations while the six Si–O_{nbr} bonds give rise to six vibrations—a total of ten vibrations per Si_2O_7 unit. The fraction of modes partitioned at the higher frequencies (i.e., 700–1100 cm^{-1}) is therefore 5/21 = 24%.

The high frequency $(Si–O_{nbr})_3$ stretching modes ranging from 800–1100 cm^{-1} can be adequately represented by one or two Einstein oscillators or a second optic continuum (Table 5: β-Mg_2SiO_4, Models 2, 3 and 5). The (Si–O_{br}) stretching frequency at 700 cm^{-1}, can be represented by an Einstein oscillator at 700 cm^{-1}. An alternative method of representing the (Si–O_{br}) and (Si–O_{nbr}) stretching modes is to place them in a second optic continuum extending from 700 to 950 cm^{-1} (Table 5: β-Mg_2SiO_4, Model 4).

Spinel, γ-Mg_2SiO_4. γ-Mg_2SiO_4 is cubic and crystallizes with the well-known spinel structure that belongs to space group *Fd3m* (Sasaki et al., 1982). The primitive unit cell is one quarter of the size of the face-centered cell and has two formula units, 14 atoms and thus 42 degrees of freedom. The volume of the primitive unit cell is 132.0 × 10^{-24} cm^3 and the Brillouin zone radius is 7.65 × 10^7 cm^{-1}.

As in the case of β-Mg_2SiO_4, data from germanate analogue compounds must be used to estimate the compressional and shear wave velocities of γ-Mg_2SiO_4 (Liebermann, 1973, 1975). Values of ν_p and ν_s are estimated to be 9.8 and 5.4 km s^{-1}, respectively. These velocities give acoustic branches that reach 255 and 140 cm^{-1} at the Brillouin zone boundary.

Features of the γ-Mg_2SiO_4 spectra (Fig. 4) noted for the lattice vibrational models are the strong absorption peaks between 800 and 840 cm^{-1} and the weaker bands ranging from 350 to 550 cm^{-1}. Because γ-Mg_2SiO_4 has high symmetry, many vibrational modes are inactive in both infrared and Raman. This lends a high uncertainty to defining the position of the lowest optic mode and thus the models for γ-Mg_2SiO_4 are less constrained than for α- or β-Mg_2SiO_4.

Watanabe's (1982) heat capacity data and an estimate of S°_{1000} based on calorimetry and phase equilibria studies were used to discriminate between "reasonable" and "outlandish" vibrational models of γ-Mg_2SiO_4. A variety of models were found to show good agreement with the experimental data (Table 5). All the models have an optic continuum spanning the lower frequency range while the high frequency Si–O stretching vibrations are represented by either an Einstein oscillator or a second continuum.

Constraints on lattice entropies

As pointed out above, there are a number of models for each polymorph which show good agreement with the available heat capacity and entropy data. Figure 5 shows

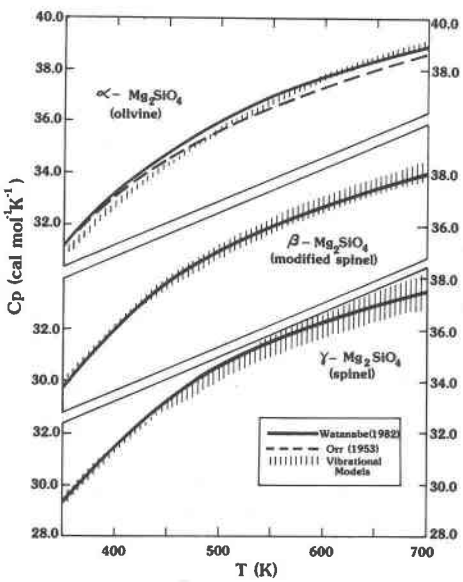

Fig. 5. Heat capacities of the Mg_2SiO_4 polymorphs as functions of temperature. Dashed curve represents Orr's (1953) forsterite data while solid curves represent experimental data from Watanabe (1982). Hatched lines represent the heat capacities estimated from vibrational models, as discussed in text.

Table 6. Standard entropies of Mg_2SiO_4 polymorphs

	S^0_{298} [a]	S^0_{700} (cal mol^{-1} K^{-1})	S^0_{1000}
Olivine (α)			
Model 3	22.75	52.42	67.04
Experimental	22.75	51.82	66.24
Modified Spinel (β)			
Models (Average)	20.89	49.80	64.20
Spinel (γ)			
Models (Average)	20.31	48.79	62.87

[a] 1 cal = 4.184 joule.

the range in C_P's predicted from the models and their agreement with the experimental C°_P data. Models predict C°_P values within 2–3% of the experimental data for each polymorph.

Entropies of the Mg_2SiO_4 polymorphs based on the vibrational models are shown in Table 6. The entropies tabulated for α-Mg_2SiO_4 are based on Model 3 (see above) which shows the best agreement with the entropy of forsterite from 300 to 1000 K. Since high temperature entropy data are available for α-Mg_2SiO_4, better constraints can be imposed on forsterite than the other two polymorphs. The entropies for β- and γ-Mg_2SiO_4 in Table 5 are based on averages of the models in Table 5 since all these models are consistent with the spectra and thermodynamic data. It is encouraging to note that these entropies from the various models are within 2% for β-Mg_2SiO_4 and 3% for γ-Mg_2SiO_4.

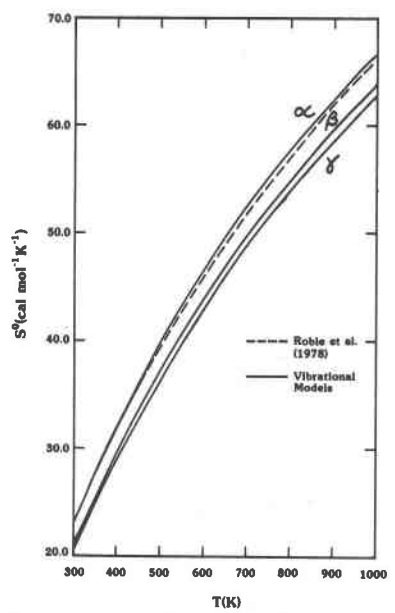

Fig. 6. Standard entropies (S°_T) of Mg_2SiO_4 polymorphs, calculated from vibrational models (solid curves), as functions of temperature. Experimental standard entropy of α-Mg_2SiO_4 (Orr, 1953; Robie et al., 1978) is shown as dashed curve.

Entropies for the Mg_2SiO_4 polymorphs are plotted as a function of temperature in Figure 6. This shows one of the advantages of the vibrational calculations—estimates of S° and C°_P can be obtained for temperatures where experimental data are not available. At high temperatures (>700 K), anharmonicity begins to play a significant role. Thermal expansion data and bulk modulus values used in the correction of C_V to C_P are listed in Table 3. At 1000 K, this correction increases the entropy by roughly 0.3 to 0.5%.

The entropies of transition at 1000 K based on the vibrational calculations for $\alpha \rightarrow \beta$ and $\beta \rightarrow \gamma$ are -2.8 ± 0.6 and -1.3 ± 0.9 cal mol^{-1} K^{-1}, respectively. These compare well with the ΔS° values based on the combination of calorimetry and phase equilibria data which give -2.5 ± 0.5 cal mol^{-1} K^{-1} for the $\alpha \rightarrow \beta$ transition and -1.5 ± 0.9 cal mol^{-1} K^{-1} for the $\beta \rightarrow \gamma$ transition.

Conclusions—utility of vibrational modelling

This study has shown that a range of reasonable vibrational models can be obtained for the Mg_2SiO_4 polymorphs from the appropriate crystallographic, acoustic shear wave, and spectral data. Heat capacities and entropies estimated by the models are found to be in good agreement with available experimental data. In addition, models which predict heat capacities within 2–3% of the measured values at 298–700 K also predict entropies which fall within a range of about 3%. That is, although the vibrational models may differ in details such as the choice of dispersion constants, optic continua versus Einstein oscillators, and partitioning of the modes, the calculated entropies are not overly sensitive to these details.

The consistency of the vibrational and thermochemical estimates of entropies encourages us to attempt similar vibrational calculations for other phases occurring at even higher pressures; e.g., silicate ilmenites, perovskites and garnets. The amount of material needed for infrared and Raman spectroscopy is much smaller than that needed for solution calorimetry. Thus vibrational calculations may provide constraints on the entropies of such transitions when no other data can be obtained. Using such an approach, with very crude estimates of the spectra of $MgSiO_3$ ilmenite and perovskite, we predict a negative P–T slope for the ilmenite → perovskite transition. However, this preliminary calculation needs further refinement and better spectral data.

Acknowledgments

This work was supported by National Science Foundation Grant DMR 8106027. We offer heartfelt thanks to S. Akimoto and E. Ito, without whose assistance and facilities the β- and γ-Mg_2SiO_4 samples would not have been made. We thank S. W. Kieffer for encouragement, discussion, explanation, and assistance in the vibrational calculations, G. Rossman for help with infrared spectroscopy and the Center for Solid State Science at Arizona State University for the use of their Raman facility.

M. A. is grateful to Kanazawa University for granting him a leave of absence. We thank R. Jeanloz for helpful comments and R. C. Liebermann and an anomymous reviewer for constructive review. We thank H. Sawamoto for providing new data on the β-γ transition and S. Sasaki for discussion of the stability of γ-Mg_2SiO_4.

References

Akimoto, S., Matsui, Y., and Syono, Y. (1976) High pressure crystal chemistry in orthosilicates and formation of the mantle transition zone. In R. G. J. Strens, Ed., The Physics and Chemistry of Minerals and Rocks, p. 327–364. Wiley, London.

Brown, G. E. (1980) Olivines and silicate spinels. In P. H. Ribbe, Ed., Reviews in Mineralogy, Vol. 5, Orthosilicates, p. 275–381, Mineralogical Society of America, Washington, D.C.

Charlu, T. V., Newton, R. C., and Kleppa, O. J. (1975) Enthalpy of formation at 975 K of compounds in the system MgO–Al_2O_3–SiO_2 from high temperature solution calorimetry. Geochimica et Cosmochimica Acta, 39, 1487–1497.

Fateley, W. G., Dollish, F. R., McDevitt, N. T., and Bentley, F. F. (1972) Infrared and Raman selection rules for molecular and lattice vibrations: the correlation method. Wiley-Interscience, New York.

Fukizawa, A. (1982) Direct determinations of phase equilibria of geophysically important materials under high pressures and high temperatures using in situ x-ray diffraction method. Ph.D. Thesis, Univ. of Tokyo.

Graham, E. K. and Barsch, G. R. (1969) Elastic constants of single crystal forsterite as a function of temperature and pressure. Journal of Geophysical Research, 75, 5949–5960.

Hazen, R. M. (1976) Effect of temperature and pressure on the crystal structure of forsterite. American Mineralogist, 61, 1280–1293.

Horiuchi, H. and Sawamoto, H. (1981) β-Mg_2SiO_4: Single-crystal X-ray diffraction study. American Mineralogist, 66, 568–575.

Iishi, K. (1978) Lattice dynamics of forsterite. American Mineralogist, 63, 1198–1208.

Ito, E., Matsui, Y., Suito, K., and Kawai, N. (1974) Synthesis of γ-Mg_2SiO_4. Physics of the Earth and Planetary Interiors, 8, 342–344.

Jeanloz, R. (1980) Infrared spectra of olivine polymorphs: α, β-phase and spinel. Physics and Chemistry of Minerals, 5, 327–339.

Jeanloz, R. and Thompson, A. B. (1983) Phase transitions and mantle discontinuities, Review of Geophysics and Space Physics, 21, 51–74.

Kawada, K. (1977) The system Mg_2SiO_4–Fe_2SiO_4 at high pressures and temperatures and the earth's interior. Ph.D. Thesis, University of Tokyo, Institute for Solid State Physics.

Kieffer, S. W. (1979a) Thermodynamics and lattice vibrations of minerals: 1. Mineral heat capacities and their relationships to simple lattice vibrational models. Reviews of Geophysics and Space Physics, 17, 1–19.

Kieffer, S. W. (1979b) Thermodynamics and lattice vibrations of minerals: 2. Vibrational characteristics of silicates. Reviews of Geophysics and Space Physics, 17, 20–34.

Kieffer, S. W. (1979c) Thermodynamics and lattice vibrations of minerals: 3. Lattice dynamics and an approximation for minerals with application to simple substances and framework silicates. Reviews of Geophysics and Space Physics, 17, 35–58.

Kieffer, S. W. (1980) Thermodynamics and lattice vibrations of minerals: 4. Application to chain and sheet silicates and orthosilicates. Reviews of Geophysics and Space Physics, 18, 862–886.

Kumazawa, M. and Anderson, O. L. (1969) Elastic moduli, pressure derivatives and temperature derivatives of single crystal olivine and single crystal forsterite. Journal of Geophysical Research, 74, 5961–5972.

Liebermann, R. C. (1973) Elastic properties of germanate analogues of olivine, spinel, and β polymorphs of $(Mg,Fe)_2SiO_4$. Nature, Physical Sciences, 244, 105–106.

Liebermann, R. C. (1975) Elasticity of olivine (α), beta (β), and spinel (γ) polymorphs of germanates and silicates. Geophysical Journal of the Royal Astronomical Society, 42, 899–929.

Mizukami, S., Ohtani, A., and Kawai, N. (1975) High-pressure X-ray diffraction studies on β- and γ-Mg_2SiO_4. Physics of the Earth and Planetary Interiors, 10, 177–182.

Morimoto, N., Tokonami, M., Watanabe, M., and Koto, K. (1974) Crystal structure of three polymorphs of Co_2SiO_4. American Mineralogist, 59, 475–485.

Navrotsky, A. (1973) Ni_2SiO_4—Enthalpy of the olivine–spinel transition by solution calorimetry at 713 °C. Earth and Planetary Science Letters, 19, 471–475.

Navrotsky, A. (1977) Recent progress in high temperature calorimetry. Physics and Chemistry of Minerals, 2, 89–104.

Navrotsky, A., Pintchovski, F. S., and Akimoto, S. (1979) Calorimetric study of the stability of high pressure phases in the systems CoO–SiO_2 and "FeO"–SiO_2 and calculation of phase diagrams in MO–SiO_2 systems. Physics of the Earth and Planetary Interiors, 19, 275–292.

Navrotsky, A., Hon, R., Weill, D. F., and Henry, D. J. (1980) Thermochemistry of glasses and liquids in the systems $CaMgSi_2O_6$–$CaAl_2Si_2O_8$–$NaAlSi_3O_8$, SiO_2–$CaAl_2Si_2O_8$–$NaAlSi_3O_8$, and SiO_2–Al_2O_3–CaO–Na_2O. Geochimica et Cosmochimica Acta, 44, 1409–1423.

Oehler, O. and Günthard, H. H. (1969) Low-temperature infrared spectra between 1200 and 20 cm^{-1} and normal-coordinate analysis of silicates with olivine structures. Journal of Chemical Physics, 51, 4719–4728.

Orr, R. L. (1953) High temperature heat contents of magnesium orthosilicate and ferrous orthosilicate. Journal of the American Chemical Society, 75, 528–529.

Piriou, B. and McMillan, P. (1983) The high-frequency vibrational spectra of vitreous and crystalline orthosilicates. American Mineralogist, 68, 426–443.

Robie, R. A., Hemingway, B. S., and Fisher, J. R. (1978) Thermodynamic properties of minerals and related substances at 298.15 K and 1 bar (10^5 pascals) pressure and at higher temperatures. U.S. Geological Survey Bulletin 1452.

Sasaki, S., Prewitt, C. T., Sato, Y., and Ito, E. (1982) Single crystal X-ray study of γ-Mg_2SiO_4. Journal of Geophysical Research, 87, 7829–7832.

Sato, Y. (1970) Modified spinel structure and its geophysical significance. M.S. Thesis, University of Tokyo, Institute of Solid State Physics.

Servoin, J. L. and Piriou, B. (1973) Infrared reflectivity and Raman scattering of Mg_2SiO_4 single crystal. Physica Status Solidi, 55, 677–686.

Smyth, J. R. and Hazen, R. M. (1973) The crystal chemistry of forsterite and hortonolite at several temperatures up to 900°. American Mineralogist, 58. 588–593.

Suito, K. (1977) Phase relations of pure Mg_2SiO_4 up to 200

kilobars. In M. Manghnani and S. Akimoto, Eds., High Pressure Research—Applications to Geophysics, p. 255–266. Academic Press, New York.

Suzuki, I. (1975) Thermal expansion of periclase and olivine and their anharmonic properties. Journal of Physics of the Earth, 23, 145–159.

Suzuki, I., Ohtani, E., and Kumazawa, M. (1979) Thermal expansion of γ-Mg_2SiO_4. Journal of Physics of the Earth, 27, 53–61.

Suzuki, I., Ohtani, E., and Kumazawa, M. (1980) Thermal expansion of modified spinel, β-Mg_2SiO_4. Journal of Physics of the Earth, 28, 273–280.

Watanabe, H. (1982) Thermochemical properties of synthetic high pressure compounds relevant to the Earth's mantle. In S. Akimoto and M. H. Manghnani, Eds., High Pressure Research in Geophysics, p. 441–464. Center for Academic Publications, Tokyo, Japan.

White, W. B. (1975) Structural interpretation of lunar and terrestrial minerals by Raman spectroscopy. In C. Karr, Jr., Ed., Infrared and Raman Spectroscopy of Lunar and Terrestrial Minerals, p. 325–358. Academic, New York.

White, W. B. and DeAngelis, B. A. (1967) Interpretation of the vibrational spectra of spinels. Spectrochimica Acta, 23A, 985–995.

Wood, B. J. and Kleppa, O. J. (1981) Thermochemistry of the forsterite-fayalite olivine solutions. Geochimica et Cosmochimica Acta, 45, 529–534.

Yagi, T. and Akimoto, S. (1976) Direct determination of the coesite-stishovite transition by in-situ X-ray measurements. Tectonophysics, 35, 259–270.

Manuscript received, March 23, 1983;
accepted for publication, December 27, 1983.